

Novel interpretation of recent experiments on the dynamics of domain walls along ferrimagnetic strips

Eduardo Martínez¹, Víctor Raposo¹ and Óscar Alejos²

¹Dpto. Física Aplicada, Universidad de Salamanca, 37008 Salamanca, Spain

²Dpto. Electricidad y Electrónica, Universidad de Valladolid, 47011 Valladolid, Spain

E-mail: oscar.alejos@uva.es

May 2020

Abstract. Domain wall motion along ferrimagnets is evaluated using micromagnetic simulations and a collective-coordinates model, both considering two sublattices with independent parameters. Analytical expressions are derived for strips on top of either a heavy metal or a substrate with negligible interfacial Dzyaloshinskii-Moriya Interaction. The work focuses its findings in this latter case, with a field-driven domain wall motion depicting precessional dynamics which become rigid at the angular momentum compensation temperature, and a current-driven dynamics presenting more complex behavior, depending on the polarization factors for each sublattice. Importantly, our analyses provide also novel interpretation of recent evidence on current-driven domain wall motion, where walls move either along or against the current depending on temperature. Besides, our approach is able to substantiate the large non-adiabatic effective parameters found for these systems.

Keywords: Micromagnetics, Domain wall dynamics, Ferrimagnets, Spin-transfer torque.
Submitted to: *Nanotechnology*

1. Introduction

Recent studies[1, 2, 3, 4, 5, 6] have focused the attention on ferrimagnets (FiMs) as feasible candidates to implement racetrack memories,[7] due to the high domain wall (DW) velocities, of the order of $1 \frac{\text{km}}{\text{s}}$, that can be reached along magnetic strips.[1, 2] Besides, such velocities linearly increase with the applied stimuli,[1, 2, 4] in the form of either magnetic fields or electric currents. These features occur at a temperature near that of angular momentum compensation T_A , when FiMs present residual net magnetization together with a null angular momentum. FiMs, as formed by two antiferromagnetically coupled ferromagnetic (FM) sublattices (SLs), possess a magnetization dependence on temperature that can be inferred from those of each SL,

$M_{s,1}(T)$ and $M_{s,2}(T)$. These temperature dependences, as plotted in the graph of FIG.1(a), can be described by expressions:

$$M_{s,i}(T) = M_{s,i}^0 \left(1 - \frac{T}{T_C}\right)^{a_i}, \quad (1)$$

where T_C is the Curie temperature of the FiM, $M_{s,i}^0$ are the magnetization of each SL at zero temperature, and a_i are certain exponents. Magnetizations of both FM SLs are equal at the temperature of magnetization compensation T_M , and this temperature can differ from T_A due to distinct Landé factors g_i for each SL.

Two different structures have been proposed to hold such fast dynamics. FiM strips grown on top of a heavy metal (HM), shown in FIG.1(b), are the first ones. The interface here provokes interfacial asymmetric exchange interactions, as the interfacial Dzyaloshinskii-Moriya interaction (iDMI), resulting in the formation of chiral DWs. Current driven domain wall motion (CDDWM) is then promoted by spin orbit torques (SOTs).[2, 3, 4] In the second structures, shown in FIG.1(c), FiM strips lie on a conventional substrate. The absence of iDMI interactions allows the formation of achiral DWs, whose dynamics have been characterized in both the field-driven and current-driven cases.[1, 6] Spin-transfer torques (STTs) are thought to be responsible for the CDDWM in these systems.

Most of these experimental results have been interpreted in terms of effective models, which describe FiMs as effective FMs. Within these models, the effective gyromagnetic ratio γ_i and Gilbert damping parameter α_i diverge at T_A .[8] However, other experimental studies have shown that Gilbert damping remains constant over a wide temperature range around both T_M and T_A .[5] Importantly, the underlying physics governing the DW dynamics is also missing. Alternatively, a model considering FiMs as formed by two FM SLs coupled through an interlattice exchange interaction, i.e., a two sublattice model (TSLM), can be proposed.[9, 10] Two Landau-Lifshitz-Gilbert equations are posed, one for each SL, along with an exchange interaction term between the two SLs. As an advantage over effective models, fixed values for the parameters involved in the model can be chosen, based on the experimental evidence. Particularly, this work shows how the TSLM yields a novel and more plausible interpretation of the observations of very recent results[6] on CDDWM in FiMs, where this motion can occur along or against the current depending on temperature. Besides, a key to substantiate the relatively large non-adiabatic parameters found in these materials is provided by means of positive non-adiabatic parameters and different spin polarization of the two sublattices. The TSLM can be implemented using micromagnetic (μ M) simulations or as a collective coordinate model (CCM) and it is briefly set out in the following section.

2. Models

The system is described using two unit vectors \vec{m}_i , ($i = 1, 2$) accounting for the local orientation of the magnetization of each SL, as shown in FIG.1(d). The in-plane components of these vectors provide information about the orientation of magnetic

moments within the DW through the ψ_i angles. The uniaxial anisotropy promotes the formation of domains with out-of-plane magnetization, and the magnetization transitions within any DW can be either from up-to-down (UD) or from down-to-up (DU). FIG.1(e) depicts schematically a DW in the system. Both SL are represented, one on top of the other. The transition is of UD (DU) type for the SL on top (below), due to the antiferromagnetic coupling. The individual or combined application of out-of-plane fields B_z and longitudinal currents J_x promote DW displacements along the longitudinal direction of the FiM strip, with velocity v . During the dynamics, the magnetic moments within the DW change their orientations and can reach either a steady orientation or a precessing behavior. Importantly, the complete TSLM admits misalignments between SLs, of particular interest when steady orientations are reached.[9] Nevertheless, a reduced version of the TSLM is to be adopted here, since the large antiferromagnetic coupling between SLs promotes $\psi_2 + \pi \approx \psi_1 = \psi$. Besides, precession of magnetic moments occurs with identical steady frequencies, i.e., $\dot{\psi}_{1,st} = \dot{\psi}_{2,st} = \omega_{st}$.

In this reduced version, B_z and J_x are the model inputs, and v and ω_{st} are its outputs. To distinguish between the effect of STTs and SOTs, the terms J_{FiM} , standing for the current through the FiM, in the former case, and J_{HM} , representing the current through the HM, in the latter, will be used instead of J_x . Details of the model are in the appendices A to D and elsewhere.[9, 10] The following CCM expressions are derived:

$$(\alpha_1 s_1 + \alpha_2 s_2) \frac{v}{\Delta} + Q \delta_s \omega_{st} = -(\beta_1 p_1 + \beta_2 p_2) \frac{J_{FiM}}{\Delta} - Q \frac{\pi}{2} \frac{q_1 + q_2}{t_{FiM}} J_{HM} \cos \psi + Q M B_z, \quad (2)$$

$$-Q \delta_s \frac{v}{\Delta} + (\alpha_1 s_1 + \alpha_2 s_2) \omega_{st} = Q (p_1 - p_2) \frac{J_{FiM}}{\Delta} + \frac{1}{2} B_m M \sin 2\psi + Q B_D M \sin \psi. \quad (3)$$

The parameters involved in these expressions are largely used in the literature: the net magnetization $M = M_{s,1} - M_{s,2}$, $M_{s,i}$ ($i = 1, 2$) being the saturation magnetization for each SL, $\gamma_i = \frac{g_i \mu_B}{\hbar}$ are the gyromagnetic ratios, μ_B and \hbar being respectively the Bohr magneton and the Plank constant, $s_i = \frac{M_{s,i}}{\gamma_i}$ are the SL angular momenta, $\delta_s = s_1 - s_2$ is the net angular momentum, p_i are the spin conversion factors,[6] related to the STT spin polarization values P_i through $p_i = \frac{\hbar}{2e} P_i$, e is the absolute electron charge, β_i are the non-adiabatic STT parameters, q_i are equivalent to p_i for SOTs, that is, $q_i = \frac{\hbar}{2e} \theta_{SH,i}$, where $\theta_{SH,i}$ are the spin-Hall angles. Q defines the DW transition type in the first SL, i.e., $Q = +1(-1)$ for an UD(DU) transition, and t_{FiM} is the FiM thickness, as shown in FIG.1(b). Δ , representing the DW width (see FIG.1(b) and (c)), can be taken as an additional parameter, or obtained from analytical estimations.[11] Finally, two additional fields must be defined at this point: B_m , representing the magnetostatic interactions, and B_D , which accounts for the asymmetric exchange interactions. According to the discussion in Appendix C, $B_m = \mu_0 (N_x - N_y) M$ and $B_D = \frac{\pi}{2} \frac{D_1 + D_2}{M \Delta}$, where N_x and N_y are respectively the longitudinal and transverse demagnetizing factors for the DW, and D_i represent the iDMI constants for each SL.

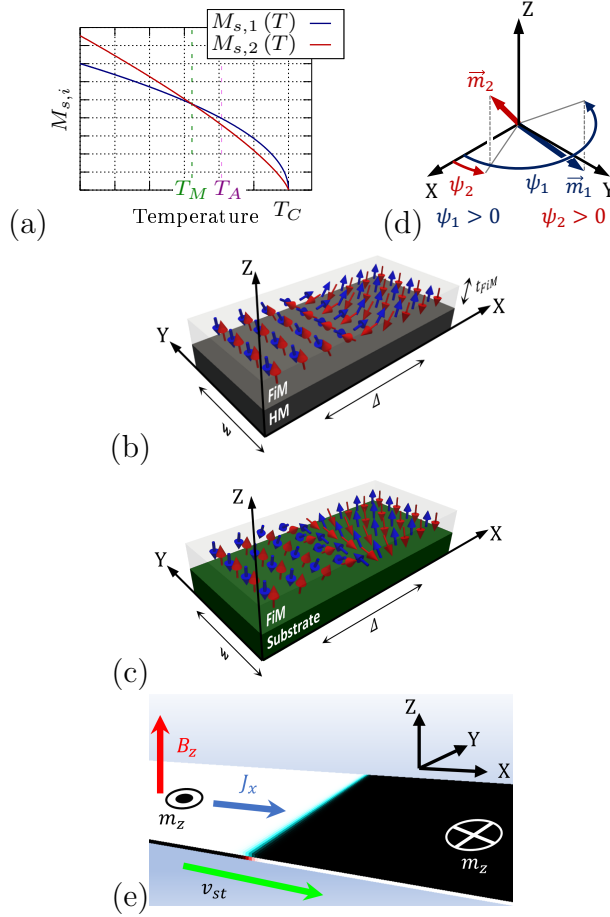


Figure 1. Two SLs constitute the FiM: (a) temperature dependence of the magnetization of each SL, (b) magnetic DW of Néel type, and (c) magnetic DW of Bloch type amidst two domains oriented out of plane (the strip width w is here shown), (d) magnetizations are represented by the unit vectors \vec{m}_1 and \vec{m}_2 , with in-plane orientation angles ψ_1 and ψ_2 , respectively, and (e) schematic representation of inputs and outputs of the TSLM.

Images (a), (b) and (c) reprinted from: E. Martínez, V. Raposo, and Ó. Alejos, AIP Advances 10, 015202 (2020); licensed under a Creative Commons Attribution (CC BY) license.

The μ M simulations presented in this work have been carried out with a homemade code[12] implemented on graphic processing units (GPUs), whereas the CCM version has been implemented by means of a conventional programming language. A comprehensive list of the parameters used for the simulations is presented below. The choice of these parameters has been made based on the values found in the literature.[2] Except if the contrary is indicated, the listed values have been adopted for all simulations. The values $T_C = 450\text{K}$, $M_{s,1}^0 = 1.4 \frac{\text{MA}}{\text{m}}$, $M_{s,2}^0 = 1.71 \frac{\text{MA}}{\text{m}}$, $a_1 = 0.5$, and $a_2 = 0.76$ have been considered. Landé factors for each SL are $g_1 = 2.2$ and $g_2 = 2$. Accordingly, the compensation temperature and the temperature of angular momentum compensation can be estimated as $T_M = 241.5\text{K}$ and $T_A = 305\text{K}$, respectively. Besides, the following values have been taken for both SLs: Gilbert damping constants are $\alpha_i = 0.02$,[5]

exchange interactions are set to $A_i = 70 \frac{\text{pJ}}{\text{m}}$, and out-of-plane crystalline anisotropy constants take the value $k_{u,i} = 1.5 \frac{\text{MJ}}{\text{m}^3}$. According to the discussion in Appendix D, the domain wall width can be estimated from these parameters as $\Delta \approx 7 \text{ nm}$. The last common parameter for all simulations is the antiferromagnetic coupling between SLs, given by an interlattice exchange constant $B_{12} = 9 \frac{\text{MJ}}{\text{m}^3}$.[13]

The following parameters are specific for CDDWM simulations.[10] The non-adiabatic STT parameters have been made equal to the Gilbert damping, i.e., $\beta_i = 0.02$. The simulations where both polarization factors are equal have been carried out with $P_1 = P_2 = 0.7$. Oppositely, the simulations where both polarization factors differ each other have been carried out with $P_1 = 0.8$ and $P_2 = 0.6$.

3. Results

3.1. Ferrimagnets grown on top of a heavy metal

This section has been included to give some completeness to the work, since most findings concerning systems dominated by spin-orbit torques have already been published by our group.[9] In particular, if iDMI exists, $B_D \gg B_m$ usually, and the TSLM confirms SOTs and iDMI as responsible for the CDDWM in FiM strips grown on top of a HM.[2, 3, 4, 9] Dynamics are characterized by the motion of rigid DWs, i.e., $\omega_{st} \equiv 0$. From (2) and (3), DW steady velocities v_{st} are reached, which are given by the expression:

$$v_{st} = \frac{\pi}{2} \frac{J_{HM}}{\sqrt{\left(\frac{\alpha_1 s_1 + \alpha_2 s_2}{q_1 + q_2} \frac{t_{FiM}}{\Delta}\right)^2 + \left(\frac{\pi}{2} \frac{\delta_s J_{HM}}{\Delta B_D M}\right)^2}}. \quad (4)$$

The above equation, not included in our previous works, constitutes a closed-form expression that summarizes DW dynamics in these systems. According to this result, the v_{st} saturate as the electric current is increased, except at T_A (δ_s vanishes), where the v_{st} linearly increase with J_{HM} because DW magnetic moments keep aligned with the electric current. DW terminal velocities maximize at this temperature, so that $v_{st} = \frac{\pi}{2} \frac{q_1 + q_2}{\alpha_1 s_1 + \alpha_2 s_2} \frac{\Delta}{t_{FiM}} J_{HM}$.

3.2. Ferrimagnets grown on top of a substrate with no iDMI

More intriguing is the case of the second FiM structure shown in FIG.1(c), when iDMI vanishes. Dynamics, both field-driven and current-driven, are now dominated by precessional regimes. Mean values of v (\bar{v}) must be considered within these regimes. Precessional regimes are due to rather low magnetostatic interactions, as discussed below. Breakdown conditions can be derived from (2) and (3). For applied fields, field-driven DW motion (FDDWM) results in precessional DW displacements if the field B_z is above the value:

$$B_W = 2 \frac{\alpha_1 s_1 + \alpha_2 s_2}{|\delta_s|} B_m. \quad (5)$$

This expression recalls the Walker field for FMs,[14] but adds a factor depending inversely on δ_s . The expression generalizes that obtained in the literature from an effective model,[15] where Gilbert damping values are taken as identical for both SL, and diverge at T_A . FIG.2 presents \bar{v} as functions of B_z at different temperatures, obtained with the set of parameters detailed above. Only at T_A , \bar{v} increases linearly with B_z . At other temperatures, the slopes of the curves reduce when the field exceeds the corresponding B_W at the given temperature. Resulting B_W values are of a few mT or less, except at T_A , where B_W diverges, as schematically shown in the inset plot.

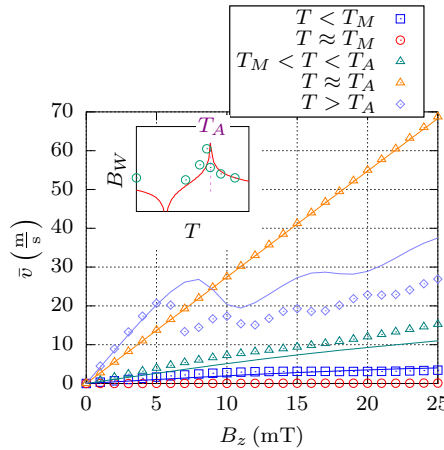


Figure 2. Dependence of \bar{v} as functions of B_z at different temperatures. Absolute values of \bar{v} have been considered since the net magnetization change sign below and above T_M , resulting respectively in negative and positive velocities if the sign of the net magnetization is taken into account. Dots represent the values obtained from μM simulations and continuous lines correspond to CCM results. The change in slope of the curves reveals the transition from a non-precessional to a precessional dynamic at a certain applied field B_W . This fact defines the condition posed to determine B_W as the points at which the linearity between velocities and applied stimuli disappears. Such points are close to local velocity maxima. The inset compares the B_W (in log scale) obtained from μM simulations (dots) and the CCM (continuous lines).

A similar analysis can be performed regarding CDDWM. In particular, the threshold current J_W leading to precessional CDDWM can be worked out as:

$$J_W = \frac{2(\alpha_1 s_1 + \alpha_2 s_2) M \Delta}{|\delta_s (\beta_1 p_1 + \beta_2 p_2) + (\alpha_1 s_1 + \alpha_2 s_2) (p_1 - p_2)|} B_m. \quad (6)$$

This expression is fully consistent with that of FMs.[14] Indeed, the TSLM provides the correct expression for FMs if ferromagnetic coupling between SLs is considered.

Two scenarios can be observed here. First, if both polarization values are equal ($P_1 = P_2$), the denominator of (6) vanishes at T_A , resulting in CDDWM sharing the same characteristics than FDDWM around this temperature. The CDDWM lacks of adiabatic contributions, as defined by Okuno and coworkers,[6] i.e., the term multiplying J_{FiM} in (3). This is shown in FIG.3. Absolute values of \bar{v} are presented because CDDWM runs in the opposite direction to the electric current with the adopted set of parameters (positive non-adiabatic STTs).

When $(P_1 \neq P_2)$, J_W does not diverge in general, even at T_A , due to the adiabatic STT contributions. Rather low electric currents promote DW precessional behavior. J_W is of the order of one ten of $\frac{G_A}{m^2}$ around T_A for the set of parameters used. More interestingly, CDDWM can take place in either the same or the opposite direction of the electric current depending on temperature. All this is depicted in FIG.4.

Previous analysis demonstrates that precessional regimes dominate DW motion in FiMs grown on substrates with no iDMI in most practical situations. Within this regime \bar{v} and ω_{st} can be estimated from (2) and (3) as:

$$\frac{\bar{v}}{\Delta} = Q \frac{(\alpha_1 s_1 + \alpha_2 s_2) M}{(\alpha_1 s_1 + \alpha_2 s_2)^2 + \delta_s^2} B_z - \frac{(\alpha_1 s_1 + \alpha_2 s_2) (\beta_1 p_1 + \beta_2 p_2) + \delta_s (p_1 - p_2)}{(\alpha_1 s_1 + \alpha_2 s_2)^2 + \delta_s^2} \frac{J_{FiM}}{\Delta}, \quad (7)$$

$$\omega_{st} = \frac{\delta_s M}{(\alpha_1 s_1 + \alpha_2 s_2)^2 + \delta_s^2} B_z + Q \frac{(\alpha_1 s_1 + \alpha_2 s_2) (p_1 - p_2) - \delta_s (\beta_1 p_1 + \beta_2 p_2)}{(\alpha_1 s_1 + \alpha_2 s_2)^2 + \delta_s^2} \frac{J_{FiM}}{\Delta}. \quad (8)$$

The expressions present linear relationships between inputs and outputs. As a first outcome, these results prove that FDDWM shows \bar{v} maxima approximately when the net angular momentum vanishes, i.e., at T_A , as evidenced by other authors.[1] Besides, these expressions also show that precession vanishes at this temperature.

The second conclusion that can be extracted from (7) and (8) is that the most recent results presented by Okuno and coworkers[6] can be naturally explained with the use of the TSLM. In this work, the authors distinguish adiabatic and non-adiabatic components of the CDDWM, related respectively to effective Gilbert damping α and non-adiabatic STT β parameters. According to our modeling, the origin of that adiabatic term is the different spin polarizations promoted by the components of each SL.[16] The effective parameters in Okuno's model can be then obtained from these of

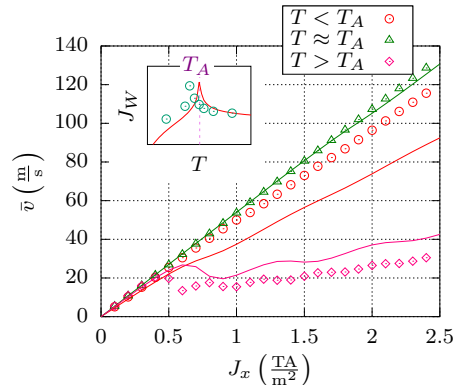


Figure 3. Dependence of absolute \bar{v} as functions of the longitudinal current J_x at different temperatures in the case $(p_1 = p_2)$. CDDWM shares in this case rather similar features to those of FDDWM. The inset presents J_W (in log scale) as a function of temperature.

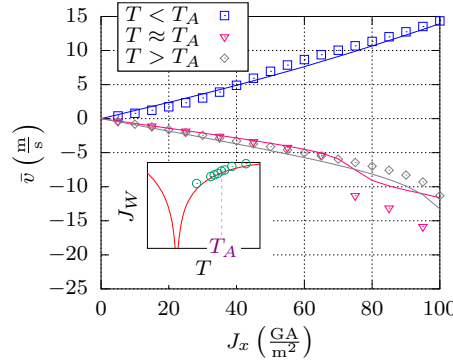


Figure 4. Dependence of \bar{v} as functions of the longitudinal current J_x at different temperatures in the case ($p_1 \neq p_2$). Depending on temperature, CDDWM runs in the same or the opposite direction to the electric current. The inset presents J_W (in log scale) as a function of temperature.

the TSLM as: $\alpha = \frac{\alpha_1 s_1 + \alpha_2 s_2}{s_1 + s_2}$ and $\beta = \frac{\beta_1 p_1 + \beta_2 p_2}{p_1 - p_2}$. While the effective α is a weighted value of the α_i for each SL, and so, rather close to the latter values, the value β diverges if the spin polarizations for each SL are quite close. This accounts for the large β needed to explain CDDWM in FiMs from the perspective of effective models.

With the TSLM, general expressions for the DW mobility over the full temperature range can also be obtained. Mobilities are defined as the ratios between \bar{v} and the inputs B_z and J_{FiM} . Despite being both stimuli simultaneously applied in that experimental work, constant mobilities can be separately studied and analyzed, due to the linear character of the system, as (7) proves. The attention will be now focused on CDDWM, and its corresponding mobility term μ . This term is calculated in the experimental work as $\mu = \frac{\bar{v}(B_z, J_{FiM}) - \bar{v}(B_z, -J_{FiM})}{2J_{FiM}}$. Because of the linear behavior, this term can be simply computed as $\mu = \frac{\bar{v}(0, J_{FiM})}{J_{FiM}} = -\frac{(\alpha_1 s_1 + \alpha_2 s_2)(\beta_1 p_1 + \beta_2 p_2) + \delta_s(p_1 - p_2)}{(\alpha_1 s_1 + \alpha_2 s_2)^2 + \delta_s^2}$. Importantly, this parameter changes sign depending on temperature. Accordingly, CDDWM reverses around a temperature in the vicinity of T_A , i.e., DW motion takes place in the same or the opposite direction to the electric current depending on temperature. This is shown in FIG.5, where \bar{v} are plotted as functions of temperature for different electric currents. At temperatures below (above) approximately T_A , DW motion takes place along (oppositely) the direction of the electric current. Constant mobility can be checked in the inset plot, where μ is computed in the four cases considered, since all computed graphs accurately superpose. The curves plotted in FIG.5 adequately emulates the aforementioned experimental results.[6] It must be noted that together with different polarization factors for each sublattice, our results were obtained by assuming positive non-adiabatic parameters. Indeed, the explanation of the experimental results[6] were based on an effective model that requires a negative non-adiabatic parameter, which lacks of experimental verification.

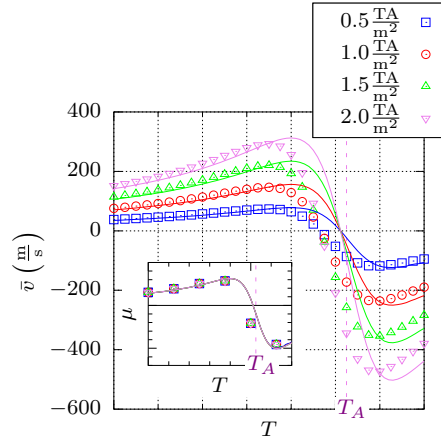


Figure 5. Dependence of \bar{v} as functions of temperature for different applied currents in the case ($p_1 \neq p_2$). Depending on temperature, CDDWM runs in the same or the opposite direction to the electric current. The inset presents the DW mobility μ as a function of temperature.

4. Conclusions

To conclude, the present analysis highlights the capabilities of the TSLM to explain very recent evidence on DW motion in FiM strips. Two different structures have been considered. In the case of FiMs grown on top of a HM, where SOTs dominate the CDDWM, a brief review of the relevant features of these dynamics is made. In these first structures, v_{st} present maxima when net angular momenta vanishes at T_A . The second structure, where FiMs are grown on a substrate with no iDMI, is characterized by richer DW dynamics. Precession dominates such dynamics in most practical situations. In particular, the angular momentum compensation results in \bar{v} maximizing around T_A for the FDDWM. Besides, CDDWM presents adiabatic and non-adiabatic contributions. The adiabatic term results from the different spin polarizations[16] promoted by the components of either SL. As this difference reduces, the adiabatic term vanishes. This fact explains why large non-adiabatic parameters are required to interpret the experimental results in these structures from the perspective of effective models. The prevalence of the non-adiabatic term over the adiabatic one results in CDDWM more similar to FDDWM. Last but not least, the TSLM has successfully interpreted novel experiments, where CDDWM can take place in one or the opposite direction depending on temperature. This change in the dynamics occurs near T_A . Accordingly, the TSLM has been proved to be a primary tool to deduce in the near future the key material parameters governing experimental observations.

Acknowledgments

This work was partially supported by Project No. MAT2017-87072-C4-1-P from the (Ministerio de Economía y Competitividad) Spanish Government and Project No.

SA299P18 from the (Consejería de Educación of) Junta de Castilla y León.

The data that supports the findings of this study are available within the article.

Appendix A. Calculation of the demagnetizing energy

The demagnetizing energy in the TSLM is calculated from the description of the magnetization textures by means of some collective coordinates. Such collective coordinates are the instantaneous position q of a domain wall (DW) in the system, and the orientations ψ_i of the in-plane components of the DW moments of each sublattice (SL) with respect to the longitudinal axis (X-axis) of the strip. The local magnetization of each SL, given by their respective saturation values M_s and two unit vectors \vec{m}_i defining their local orientation by means of their polar angles θ_i and azimuthal angles ϕ_i , is then written as functions of these collective coordinates through the well-known ansatz $\theta_i = 2Q_i \arctan\left(\frac{x-q}{\Delta}\right)$ and $\phi_i = \psi_i$, Δ accounting for the DW width, and Q_i determining the magnetization transition, as they have been defined in the main text. The approach that both SLs share the same position q and width Δ has been made here, which seems to be valid even for slightly weak coupling between SLs.[12] Additionally, Δ can be estimated from the other model parameters, as it will be discussed in Appendix D. Before the application of the ansatz, the demagnetizing energy can be expressed as:

$$\epsilon_m = \frac{1}{2}\mu_0 (M_{s,1}\vec{m}_1 + M_{s,2}\vec{m}_2) \begin{pmatrix} N_x & 0 & 0 \\ 0 & N_y & 0 \\ 0 & 0 & N_z \end{pmatrix} (M_{s,1}\vec{m}_1 + M_{s,2}\vec{m}_2)^T, \quad (\text{A.1})$$

μ_0 being the vacuum permeability and N_x , N_y and N_z representing the demagnetizing factors given by the DW dimensions. From (A.1) and the use of the ansatz, the density energy per unit area σ_m is computed as:

$$\sigma_m = \int_{-\infty}^{\infty} \epsilon_m dx = \mu_0 \Delta \left[N_x (M_{s,1} \cos \psi_1 + M_{s,2} \cos \psi_2)^2 + N_y (M_{s,1} \sin \psi_1 + M_{s,2} \sin \psi_2)^2 - N_z (M_{s,1} + Q_1 Q_2 M_{s,2})^2 \right], \quad (\text{A.2})$$

where the results $\int_{-\infty}^{\infty} \sin^2 \theta_i dx = 2\Delta$ and $\int_{-\infty}^{\infty} \cos^2 \theta_i dx = -2\Delta$ have been considered. For antiferromagnetic (ferromagnetic) coupling, it follows that $Q_1 Q_2 = -1$ (+1).

Appendix B. Calculation of the iDMI energy.

The energy density per unit area accounting for the asymmetric exchange interactions, as it is the case of the interfacial Dzyaloshinskii-Moriya interaction (iDMI), is derived in a similar fashion to the demagnetizing energy. The calculation starts from the energy density:

$$\epsilon_D = D_1 [(\hat{z} \cdot \vec{m}_1) \nabla \vec{m}_1 - (\vec{m}_1 \nabla) (\hat{z} \cdot \vec{m}_1)] + D_2 [(\hat{z} \cdot \vec{m}_2) \nabla \vec{m}_2 - (\vec{m}_2 \nabla) (\hat{z} \cdot \vec{m}_2)], \quad (\text{B.1})$$

where D_i represent the iDMI constants for each SL, and \hat{z} is the unit vector in the out-of-plane direction. Integration along the longitudinal axis of (B.1) and the use of the

ansatz results in the following area density:

$$\sigma_D = \pi Q_1 D_1 \cos \psi_1 + \pi Q_2 D_2 \cos \psi_2. \quad (\text{B.2})$$

Appendix C. Derivation of the simplified collective coordinate model (CCM) for the TSLM

The minimization of the whole functional including σ_m and σ_D goes through the calculation of its derivatives with respect to q , \dot{q} , and ψ_i and $\dot{\psi}_i$ (more details can be found in the literature[9]). This results in a system of the following three equations that make up the generalized CCM for the TSLM.

$$\begin{aligned} \frac{\dot{q}}{\Delta} (\alpha_1 s_1 + \alpha_2 s_2) + Q_1 s_1 \dot{\psi}_1 + Q_2 s_2 \dot{\psi}_2 = \\ = -(\beta_1 p_1 + \beta_2 p_2) \frac{J_{FiM}}{\Delta} + (Q_1 M_{s,1} + Q_2 M_{s,2}) B_z - \\ - \frac{\pi}{2} (Q_1 q_1 \cos \psi_1 + Q_2 q_2 \cos \psi_2) \frac{J_{HM}}{t_{FiM}}, \end{aligned} \quad (\text{C.1})$$

$$\begin{aligned} -Q_1 \frac{\dot{q}}{\Delta} s_1 + \alpha_1 \dot{\psi}_1 s_1 = \\ = Q_1 p_1 \frac{J_{FiM}}{\Delta} - \frac{1}{2} \mu_0 (N_y - N_x) M_{s,1}^2 \sin 2\psi_1 - \\ - \mu_0 M_{s,1} M_{s,2} (N_y \cos \psi_1 \sin \psi_2 - N_x \sin \psi_1 \cos \psi_2) + \\ + Q_1 \frac{\pi D_1}{2 \Delta} \sin \psi_1 - B_{ex} \sin (\psi_1 - \psi_2), \end{aligned} \quad (\text{C.2})$$

$$\begin{aligned} -Q_2 \frac{\dot{q}}{\Delta} s_2 + \alpha_2 \dot{\psi}_2 s_2 = \\ = Q_2 p_2 \frac{J_{FiM}}{\Delta} - \frac{1}{2} \mu_0 (N_y - N_x) M_{s,2}^2 \sin 2\psi_2 - \\ - \mu_0 M_{s,1} M_{s,2} (N_y \sin \psi_1 \cos \psi_2 - N_x \cos \psi_1 \sin \psi_2) + \\ + Q_2 \frac{\pi D_2}{2 \Delta} \sin \psi_2 + B_{ex} \sin (\psi_1 - \psi_2), \end{aligned} \quad (\text{C.3})$$

where all parameters have already been introduced in the main text, except B_{ex} , representing the exchange coupling between SLs.

By combining (C.2) and (C.3), a new expression can be obtained:

$$\begin{aligned} -\frac{\dot{q}}{\Delta} (Q_1 s_1 + Q_2 s_2) + \alpha_1 s_1 \dot{\psi}_1 + \alpha_2 s_2 \dot{\psi}_2 = \\ = (Q_1 p_1 + Q_2 p_2) \frac{J_{FiM}}{\Delta} - \\ - \frac{1}{2} \mu_0 (N_y - N_x) [M_{s,1}^2 \sin 2\psi_1 + M_{s,2}^2 \sin 2\psi_2 + 2M_{s,1} M_{s,2} \sin (\psi_1 + \psi_2)] + \\ + \frac{\pi}{2} \left(\frac{Q_1 D_1}{\Delta} \sin \psi_1 + \frac{Q_2 D_2}{\Delta} \sin \psi_2 \right). \end{aligned} \quad (\text{C.4})$$

Now it is time to apply the approximations mentioned in the main text, that is, $Q = Q_1 = -Q_2$ and $\psi_2 + \pi \approx \psi_1 = \psi$ ($Q = Q_1 = Q_2$ and $\psi_2 \approx \psi_1 = \psi$) for the antiferromagnetic (ferromagnetic) case. Only the antiferromagnetic case will be

considered here (the ferromagnetic one can be straightforwardly derived). In this case, (C.1) and (C.4) can be rewritten as:

$$\begin{aligned} \frac{\dot{q}}{\Delta} (\alpha_1 s_1 + \alpha_2 s_2) + Q \delta_s \dot{\psi} = \\ = -(\beta_1 p_1 + \beta_2 p_2) \frac{J_{FiM}}{\Delta} + Q M B_z - Q \frac{\pi}{2} (q_1 + q_2) \cos \psi \frac{J_{HM}}{t_{FiM}}, \end{aligned} \quad (\text{C.5})$$

$$\begin{aligned} -Q \delta_s \frac{\dot{q}}{\Delta} + (\alpha_1 s_1 + \alpha_2 s_2) \dot{\psi} = \\ = Q (p_1 - p_2) \frac{J_{FiM}}{\Delta} - \frac{1}{2} \mu_0 (N_y - N_x) (M_{s,1} - M_{s,2})^2 \sin 2\psi + \\ + Q (M_{s,1} - M_{s,2}) \frac{\pi}{2} \frac{D_1 + D_2}{(M_{s,1} - M_{s,2}) \Delta} \sin \psi. \end{aligned} \quad (\text{C.6})$$

Equations (C.5) and (2) are directly comparable. By comparison of equation (C.6) and (3), it follows the definition of the demagnetizing and iDMI fields as $B_m = \mu_0 (N_x - N_y) M$ and $B_D = \frac{\pi D_1 + D_2}{2 M \Delta}$, $M = M_{s,1} - M_{s,2}$ being the net saturation magnetization. These definitions are consistent with the equivalent expressions for pure ferromagnets.

Appendix D. Determination of the DW width

The σ_m value calculated in Appendix A also determines the analytical calculation of the DW width. In this case, the whole functional must be minimized with respect to Δ . Under the approximations above in the antiferromagnetic coupling case, the derivative of σ_m with respect to Δ yields:

$$\frac{\partial \sigma_m}{\partial \Delta} = \mu_0 (M_{s,1} - M_{s,2})^2 (N_x \cos^2 \psi + N_y \sin^2 \psi - N_z), \quad (\text{D.1})$$

which again is consistent with the corresponding expression for pure ferromagnets. Hence, it can be obtained that:

$$\Delta = \sqrt{\frac{A_1 + A_2}{k_{u,1} + k_{u,2} - \frac{1}{2} \mu_0 (M_{s,1} - M_{s,2})^2 [(N_z - N_x) + (N_x - N_y) \sin^2 \psi]}}, \quad (\text{D.2})$$

A_i and $k_{u,i}$ being respectively the exchange and uniaxial out-of-plane anisotropy constants for each SL. A slightly more accurate version of this expression can be found in the literature.[11] Alternatively, Δ can be included among the parameters of the model.

References

- [1] K.-J. Kim, S. K. Kim, Y. Hirata, S.-H. Oh, T. Tono, D.-H. Kim, T. Okuno, W. S. Ham, S. Kim, G. Go, Y. Tserkovnyak, A. Tsukamoto, T. Moriyama, K.-J. Lee, and T. Ono, “Fast domain wall motion in the vicinity of the angular momentum compensation temperature of ferrimagnets,” *Nature Materials*, vol. 16, pp. 1187–1192, 2017.
- [2] L. Caretta, M. Mann, F. Büttner, K. Ueda, B. Pfau, C. M. Günther, P. Hessing, A. Churikova, C. Klose, M. Schneider, D. Engel, C. Marcus, D. Bono, K. Baggshik, S. Eisebitt, and G. S. D. Beach, “Fast current-driven domain walls and small skyrmions in a compensated ferrimagnet,” *Nature Nanotechnology*, vol. 3, 2018.

- [3] R. Bläsing, T. Ma, S.-H. Yang, C. Garg, F. K. Dejene, A. T. N'Diaye, G. Chen, K. Liu, and S. S. P. Parkin, "Exchange coupling torque in ferrimagnetic Co/Gd bilayer maximized near angular momentum compensation temperature," *Nature Communications*, vol. 9, p. 4984, 2018.
- [4] S. A. Siddiqui, J. Han, J. T. Finley, C. A. Ross, and L. Liu, "Current-induced domain wall motion in a compensated ferrimagnet," *Physical Review Letters*, vol. 121, p. 057701, 2018.
- [5] D.-H. Kim, T. Okuno, S. K. Kim, S.-H. Oh, T. Nishimura, Y. Hirata, Y. Futakawa, H. Yoshikawa, A. Tsukamoto, Y. Tserkovnyak, Y. Shiota, T. Moriyama, K.-J. Kim, K.-J. Lee, and T. Ono, "Low magnetic damping of ferrimagnetic GdFeCo alloys," *Physical Review Letters*, vol. 122, p. 127203, 2019.
- [6] T. Okuno, D.-H. Kim, S.-H. Oh, S. K. Kim, Y. Hirata, T. Nishimura, W. S. Ham, Y. Futakawa, H. Yoshikawa, A. Tsukamoto, Y. Tserkovnyak, Y. Shiota, T. Moriyama, K.-J. Kim, K.-J. Lee, and T. Ono, "Spin-transfer torques for domain wall motion in antiferromagnetically coupled ferrimagnets," *Nature Electronics*, vol. 2, pp. 389–393, 2019.
- [7] S. S. P. Parkin, M. Hayashi, and L. Thomas, "Magnetic domain wall racetrack memory," *Science*, vol. 320, p. 190, 2008.
- [8] C. D. Stanciu, A. V. Kimel, F. Hansteen, A. Tsukamoto, A. Itoh, A. Kirilyuk, and T. Rasing, "Ultrafast spin dynamics across compensation points in ferrimagnetic GdFeCo: The role of angular momentum compensation," *Physical Review B*, vol. 73, p. 220402(R), 2006.
- [9] E. Martínez, V. Raposo, and Ó. Alejos, "Current-driven domain wall dynamics in ferrimagnets: Micromagnetic approach and collective coordinates model," *Journal of Magnetism and Magnetic Materials*, vol. 491, p. 165545, 2019.
- [10] E. Martínez, V. Raposo, and Ó. Alejos, "Current driven domain wall dynamics in ferrimagnetic strips explained by means of a two interacting sublattices model," *AIP Advances*, vol. 10, p. 015202, Jan 2020.
- [11] L. Sánchez-Tejerina, V. Puliafito, P. Khalili Amiri, M. Carpentieri, and G. Finocchio, "Dynamics of domain-wall motion driven by spin-orbit torque in antiferromagnets," *Physical Review B*, vol. 101, p. 014433, Jan 2020.
- [12] Ó. Alejos, V. Raposo, L. Sanchez-Tejerina, R. Tomasello, G. Finocchio, and E. Martinez, "Current-driven domain wall dynamics in ferromagnetic layers synthetically exchange-coupled by a spacer: A micromagnetic study," *Journal of Applied Physics*, vol. 123, p. 013901, 2018.
- [13] C. T. Ma, X. Li, and S. J. Poon, "Micromagnetic simulation of ferrimagnetic tbfecos films with exchange coupled nanophases," *Journal of Magnetism and Magnetic Materials*, vol. 417, pp. 197–202, 2016.
- [14] A. Thiaville and Y. Nakatani, "Domain-wall dynamics in nanowires and nanostrips," in *Spin Dynamics in Confined Magnetic Structures III* (B. Hillebrands and A. Thiaville, eds.), vol. 101, Springer, Berlin, Heidelberg, 2005.
- [15] S.-H. Oh, S. K. Kim, D.-K. Lee, G. Go, K.-J. Kim, T. Ono, Y. Tserkovnyak, and K.-J. Lee, "Coherent terahertz spin-wave emission associated with ferrimagnetic domain wall dynamics," *Physical Review B*, vol. 96, p. 100407(R), 2017.
- [16] R. Meservey and P. Tedrow, "Spin-polarized electron tunneling," *Physics Reports*, vol. 4, pp. 173–243, Mar 1994.